Technical Reference on Hydrogen Compatibility of Materials

Plain Carbon Ferritic Steels:
C-Mn Alloys (code 1100)

Prepared by:

B.P. Somerday, Sandia National Laboratories, Livermore CA

Editors
C. San Marchi
B.P. Somerday
Sandia National Laboratories

This report may be updated and revised periodically in response to the needs of the technical community; up-to-date versions can be requested from the editors at the address given below or downloaded at http://www.sandia.gov/matlsTechRef/. The content of this report will also be incorporated into a Sandia National Laboratory report (SAND2008-1163); the most recent version can be obtained from the link above. The success of this reference depends upon feedback from the technical community; please forward your comments, suggestions, criticisms and relevant public-domain data to:

Sandia National Laboratories
Matls Tech Ref
C. San Marchi (MS-9402)
7011 East Ave
Livermore CA 94550.

Sandia National Laboratories is a multi-program laboratory operated by Sandia Corporation, a wholly owned subsidiary of Lockheed Martin Corporation, for the U.S. Department of Energy's National Nuclear Security Administration under contract DE-AC04-94AL85000.

Technical Reference on Hydrogen Compatibility of Materials

Plain Carbon Ferritic Steels:

C-Mn Alloys (code 1100)

1. General

Carbon and alloy steels can be categorized by a variety of characteristics such as composition, microstructure, strength level, material processing, and heat treatment [1]. The carbon and alloy steel categories selected for the Technical Reference on Hydrogen Compatibility of Materials are based on characteristics of the steels as well as available data. In this chapter, the steels are distinguished by the primary alloying elements, i.e., carbon and manganese. Data on the compatibility of carbon steels with hydrogen gas exist primarily for the following alloys: A515 Gr. 70, A516 Gr. 70, A106 Gr. B, A106 Gr. C, SA 105, and the 10xx steels. In addition, a substantial amount of data has been generated for the API 5L steels, grades X42 to X80. Since a full range of properties in hydrogen gas is not available for each steel, data for all carbon steels are presented in this chapter. Although plain carbon ferritic steels exhibit some metallurgical differences, the basic trends in the data are expected to apply generally to this class of steels.

Carbon steels are attractive structural materials in applications such as pipelines because the steels can be formed and welded, and adequate mechanical properties can be achieved through normalizing heat treatments or hot rolling. The API 5L steels may contain additional alloying elements, such as small quantities of niobium and vanadium. These "microalloying" additions as well as processing through controlled rolling impart a combination of elevated strength and improved low-temperature fracture resistance.

Despite the attractive properties of carbon steels, these materials must be used judiciously in structures exposed to hydrogen gas. Hydrogen gas degrades the tensile ductility of carbon steels, particularly in the presence of stress concentrations. Additionally, hydrogen gas lowers fracture toughness, and certain metallurgical conditions can render the steels susceptible to crack extension under static loading. Hydrogen gas also accelerates fatigue crack growth, even at relatively low hydrogen gas partial pressures, suggesting that small fractions of hydrogen in gas blends must be considered in fatigue life assessments. The severity of these manifestations of hydrogen embrittlement depends on mechanical, environmental, and material variables. Variables that influence behavior in hydrogen gas include loading rate, load cycle frequency, gas pressure, gas composition, and the presence of welds. Control over these variables may allow carbon steels to be applied safely in hydrogen gas environments. For example, limiting the magnitude and frequency of load cycling can improve the compatibility of carbon steels with hydrogen gas.

This chapter presents a range of data for carbon steels in hydrogen gas, including tensile and crack growth properties. The crack growth data emphasize fracture mechanics properties, since pipeline design can benefit from defect-tolerant design principles, particularly for hydrogen environments.

1.1 Composition and microstructure

Table 1.1.1 lists the allowable composition ranges for carbon steels covered in this chapter. Table 1.1.2 summarizes the compositions and product forms of steels from hydrogen compatibility studies reported in this chapter. Table 1.1.3 details the heat treatments applied to steels in Table 1.1.2. Additionally, Table 1.1.3 includes the yield strength, ultimate tensile strength, total elongation, and reduction of area that result from the heat treatments.

1.2 Common designations

A515 Gr. 70: UNS K03103, ASTM A515 (70)
A516 Gr. 70: UNS K02700, ASTM A516 (70)
A106 Gr. B: ASTM A106 (B)
A106 Gr. C: ASTM A106 (C)
SA 105 Gr. II: ASME SA-105, ASTM A105
1020: UNS G10200, AISI 1020, ASTM A830 (1020)
1042: UNS G10420, AISI 1042, ASTM A830 (1042)
1080: UNS G10800, AISI 1080, ASTM A830 (1080)
X42: API 5L X42
X52: API 5L X52
X60: API 5L X60
X65: API 5L X65
X70: API 5L X70
X80: API 5L X80

2. Permeability, Diffusivity and Solubility

The permeability and solubility of hydrogen in 10xx carbon steels are mildly affected by carbon content and microstructure [2]. In a single study, permeation experiments were conducted on six carbon steels over the temperature range 500 to 900 K and gas pressure range 0.01 to 0.7 MPa [2]. The hydrogen permeability *vs* temperature relationships are plotted in Figure 2.1 (also listed in Table 2.1) for the normalized microstructures and show that permeability systematically decreases as carbon content increases. The difference in the permeability for 1010 steel compared to 1095 steel is about a factor of three over the entire temperature range examined.

The solubility of hydrogen in 10xx carbon steels was determined from the ratio of permeability and diffusivity [2]. Solubility *vs* temperature relationships are given in Table 2.1 and plotted in Figure 2.2 and demonstrate a trend similar to permeability, where solubility generally decreases as carbon content increases. The difference in the solubility for 1010 steel compared to 1095 steel is about a factor of two over the entire temperature range examined.

Permeability and solubility *vs* temperature relationships were reported for three different microstructures [2]: normalized, spheroidized, and quenched and tempered. The permeability was nearly identical for the three microstructures over the temperature range examined. The solubility was highest in the normalized microstructure and lowest in the quenched and tempered microstructure, but the difference was less than a factor of two over the temperature range.

The solubility is the Sievert's constant in Sievert's law and thus can be used to calculate the concentration of hydrogen in the metal lattice. At lower temperatures, hydrogen segregates to

defects in metals, and the total hydrogen concentration is the sum of hydrogen in the lattice and hydrogen at defects. The solubility relationships in Table 2.1 can be used to calculate the lattice hydrogen concentration in carbon steels but not the total hydrogen concentration. More information on calculating total hydrogen concentrations in steels at lower temperatures can be found in Ref. [3].

3. Mechanical Properties: Effects of Gaseous Hydrogen

3.1 Tensile properties

3.1.1 Smooth tensile properties

Measurement of smooth tensile properties of carbon steels in high-pressure hydrogen gas demonstrates that hydrogen degrades reduction of area but not ultimate tensile strength. Tables 3.1.1.1 and 3.1.1.2 summarize properties measured in 6.9 and 69 MPa hydrogen gas for a wide range of carbon steels [4-6]. The reduction of area measurements in hydrogen gas are remarkably consistent, where most values range from 35 to 47% independent of hydrogen gas pressure. Although these absolute values remain relatively high in hydrogen gas, the loss of reduction of area relative to values measured in air or inert gas can be as high as 50%. The most notable exception to the general reduction of area trend is the high-carbon steel 1080, which exhibits a reduction of area as low as 6% in hydrogen gas. However, the reduction of area for 1080 in nitrogen gas (14%) is also relatively low.

3.1.2 Notched tensile properties

High-pressure hydrogen severely degrades the reduction of area of carbon steels when measurements are conducted using notched specimens. In addition, hydrogen mildly reduces tensile strength in notched specimens. Table 3.1.2.1 summarizes data for a range of carbon steels tested in 6.9 MPa hydrogen gas [4]. Similar to trends from smooth specimens, the reduction of area values from notched specimens are in a consistent range (5 to 9%). However, the reduction of area loss measured from notched specimens is much more pronounced than the reduction of area loss measured from smooth specimens; e.g., the reduction of area loss from notched specimens can be as high as 80% in hydrogen gas. The reduction of notched tensile strength is generally less than 15% for specimens tested in hydrogen gas.

Measurements for notched specimens in 69 MPa hydrogen gas (Table 3.1.2.2) [7] show trends similar to measurements in 6.9 MPa hydrogen gas, however absolute values cannot be compared directly since the notch geometries are different. Nonetheless, Table 3.1.2.2 shows that hydrogen induces reduction of area losses as high as 70%. Notched tensile strength losses are as high as 25% in hydrogen gas.

3.2 Fracture mechanics

3.2.1 Fracture toughness

The fracture toughness and crack propagation resistance of carbon steels are lower in high-pressure hydrogen gas compared to properties measured in air or inert gas. Table 3.2.1.1 lists fracture toughness and crack propagation resistance results for a range of carbon steels tested in hydrogen gas up to 35 MPa pressure [5, 6, 8-11]. At a constant pressure of 6.9 MPa, the fracture toughness is degraded by as much as 50% in hydrogen gas. However, absolute fracture

toughness remains high, where most values are near 100 MPa·$m^{1/2}$. Hydrogen has a more pronounced effect on crack propagation resistance; dJ/da values measured in hydrogen gas can be 90% lower than values measured in air or inert gas.

The fracture toughness measured in hydrogen gas is sensitive to both the loading rate and gas pressure. Figure 3.2.1.1 shows that the fracture toughness for X42 steel in 4 MPa hydrogen gas is constant at displacement rates from $3x10^{-5}$ to $3x10^{-4}$ mm/s but then increases by 30% as the displacement rate increases to $3x10^{-3}$ mm/s [11]. Figure 3.2.1.2 displays the fracture toughness *vs* hydrogen gas pressure data for X42 and A516 steel from Table 3.2.1.1 [8, 9, 11]. For both sets of data, fracture toughness decreases as gas pressure increases but appears to be approaching a lower limiting value. Fracture toughness values are higher for A516 compared to X42, but this difference may be due in part to the higher loading rate for tests on A516.

Fracture toughness can depend sensitively on gas composition, as illustrated in Figure 3.2.1.3 [6]. In this figure, fracture toughness measurements are shown for X42 and X70 steels in nitrogen, methane, and hydrogen, as well as mixtures of hydrogen, methane, carbon monoxide, and carbon dioxide. The results for hydrogen and nitrogen are the same data from Table 3.2.1.1. The data in Figure 3.2.1.3 show that methane does not adversely affect fracture toughness, however a mixture of methane and hydrogen causes a reduction in fracture toughness. Furthermore, fracture toughness is not degraded in gas mixtures containing hydrogen and carbon monoxide. In these cases, carbon monoxide hinders hydrogen uptake into the steel and precludes hydrogen-assisted fracture [6], at least on the time scale of the fracture toughness test.

3.2.2 Threshold stress-intensity factor

Subcritical crack extension can occur when materials are exposed to static loading and hydrogen gas concurrently. Testing was conducted on A106 Gr. B and X70 steels to assess the resistance of these materials to subcritical cracking in 6.9 and 4.1 MPa hydrogen gas partial pressures, respectively [6, 9]. Subcritical crack extension was not detected for either steel. Similarly, testing was conducted on A516 and A106 Gr. C steels to measure the threshold stress-intensity factor for subcritical crack extension (i.e., K_{TH}) at high hydrogen gas pressures [12]. As summarized in Table 3.2.2.1., no crack extension was measured at the reported stress-intensity factors.

3.3 Fatigue

3.3.1 Low-cycle and high-cycle fatigue

No known published data in hydrogen gas.

3.3.2 Fatigue crack propagation

Hydrogen gas enhances the fatigue crack growth rate of carbon steels. Figure 3.3.2.1 shows crack growth rate (da/dN) *vs* stress-intensity factor range (ΔK) relationships for a range of carbon steels in approximately 7 MPa hydrogen gas [6, 10, 13-16]. Several general trends are apparent from the data in Figure 3.3.2.1. The fatigue crack growth rates in hydrogen become increasingly greater relative to crack growth rates in air or inert gas as ΔK increases. In the higher range of ΔK, fatigue crack growth rates are at least ten-fold greater than crack growth rates in air or inert gas. While the da/dN vs ΔK relationships in air and inert gas are remarkably similar, the da/dN

vs ΔK relationships in hydrogen are noticeably more varied. In the higher range of ΔK, crack growth rates in hydrogen can vary by more than a factor of 10.

The da/dN *vs* ΔK relationships in hydrogen gas can be affected by numerous variables, including gas pressure, load ratio, load cycle frequency, and gas composition. The effects of these variables are described in the following paragraphs.

Effect of gas pressure

Fatigue crack growth rates generally increase as hydrogen gas pressure increases [13, 16]. Figure 3.3.2.2 shows da/dN vs ΔK relationships for 1020 steel in hydrogen gas from 0.02 to 7 MPa and for SA 105 steel in hydrogen gas from 7 to 100 MPa [13, 16]. The effect of hydrogen gas pressure on crack growth rates appears to depend on ΔK. At higher ΔK, the da/dN vs ΔK relationships measured in hydrogen merge, suggesting that crack growth rates are not as sensitive to gas pressure at these ΔK levels. At lower ΔK, crack growth rates can increase by more than a factor of 10 as gas pressure increases from 0.02 MPa to 100 MPa.

The da/dN vs ΔK relationship for 1020 steel in 0.02 MPa hydrogen gas is particularly striking. At this low gas pressure (less than 1 atmosphere), the crack growth rate can be a factor of 10 greater than the crack growth rate in air. This result indicates that gases containing even low partial pressures of hydrogen may accelerate fatigue crack growth in carbon steels.

Effect of load ratio

The cyclic load ratio (R, defined as the ratio of the minimum and maximum loads in the load cycle) does not control fatigue crack growth rates in hydrogen gas [10]. Figure 3.3.2.3 shows crack growth rates measured for X42 steel in hydrogen gas as a function of load ratio at a fixed ΔK. While the crack growth rate is independent of load ratio for values between 0.1 and 0.4, the crack growth rate increases at higher load ratios. This increase in crack growth rates is controlled not by the load ratio but by the maximum stress-intensity factor (K_{max}) in the load cycle. Since $\Delta K = K_{max}(1-R)$, an increase in R at fixed ΔK requires that K_{max} increase as well. The crack growth rate accelerates at higher load ratios because K_{max} is approaching the fracture toughness in hydrogen gas (e.g., the values in Table 3.2.1.1) [10].

Although Figure 3.3.2.3 shows that crack growth rates in hydrogen gas are not a function of load ratio in the range from 0.1 to 0.4, crack growth rates in nitrogen are a strong function of load ratio. Thus, as load ratio increases from 0.1 to 0.4, hydrogen has less effect on crack growth rate relative to the crack growth rate in nitrogen. The varying effect of load ratio on crack growth rates in hydrogen and nitrogen has been attributed to crack closure. It has been suggested that plasticity-induced crack closure is less pronounced in hydrogen compared to environments such as nitrogen [10].

Other measurements of fatigue crack growth rates in hydrogen gas indicate that da/dN *vs* ΔK relationships do not depend on load ratio. The da/dN *vs* ΔK relationships for 1020 steel in 7 MPa hydrogen gas are nearly identical at load ratios of 0.15 and 0.37 [13].

Effect of load cycle frequency

Fatigue crack growth rates in hydrogen gas generally increase as the load cycle frequency decreases. This trend is illustrated in Figure 3.3.2.4, which displays da/dN *vs* ΔK relationships

for SA 105 steel in 100 MPa hydrogen gas over a range of load cycle frequencies from 0.001 to 1 Hz [16]. As frequency decreases from 1 to 0.001 Hz, the crack growth rate increases by about a factor of 5.

Additional data for SA 105 steel in 100 MPa hydrogen gas demonstrate that the load cycle profile can be important as well. Figure 3.3.2.5 shows fatigue crack growth rates plotted against the cycle duration (reciprocal of frequency) [16]. These data were generated using two different load profiles, where the time to reach maximum load was either 0.5 or 100 seconds. While the fatigue crack growth rate generally increases as the cycle duration increases, crack growth rates for the 100 second ramp appear to increase more rapidly than crack growth rates for the 0.5 second ramp.

The effect of load cycle frequency on fatigue crack growth rates in hydrogen gas has been demonstrated for other steels. Fatigue crack growth rates for 1020 steel in 0.14 MPa hydrogen gas decreased as frequency increased from 1 to 10 Hz [13].

Effect of gas composition

Additives to hydrogen gas can reduce fatigue crack growth rates, however this phenomenon has not been explored at low load cycle frequencies. Figure 3.3.2.6 shows da/dN *vs* ΔK relationships for X42 steel in 6.9 MPa hydrogen gas containing three different additives: oxygen, sulfur dioxide, or carbon monoxide [6]. In each case, the gas additive lowers the fatigue crack growth rate to the crack growth rate measured in nitrogen, at least for the relatively high frequency (1 Hz) used in the study.

The effect of hydrogen gas mixtures on fatigue crack growth was also explored for 1020 steel at a load cycle frequency of 1 Hz and low total gas pressure. Figure 3.3.2.7 shows da/dN *vs* ΔK relationships for three gas mixtures: hydrogen and carbon dioxide, hydrogen and natural gas, and hydrogen and water [17]. The addition of carbon dioxide to hydrogen has no effect on fatigue crack growth rates, as the da/dN *vs* ΔK relationship for the gas mixture is similar to the relationship for pure hydrogen. The crack growth rate in water plus hydrogen is lower than the crack growth rate in pure hydrogen; however, hydrogen plus water vapor raises the crack growth rate above the crack growth rate in pure water vapor. Finally, the crack growth rate in hydrogen plus natural gas is similar to the crack growth rate in pure hydrogen. In addition, the crack growth rate in pure natural gas is nearly the same as the crack growth rate in air.

3.4 Recent mechanical property measurements

3.4.1 Fracture toughness

The fracture toughness was measured for X60 and X80 steels in 5.5 and 21 MPa hydrogen gas [18, 19]. Although fracture toughness values were notably higher for the X80 steel compared to the X60 steel (Table 3.2.1.1), values for both steels were comparable to others listed in Table 3.2.1.1, i.e., near 100 $MPa \cdot m^{1/2}$. The varying hydrogen gas pressure did not significantly affect fracture toughness for either the X60 steel or the X80 steel.

3.4.2 Fatigue crack propagation

Figure 3.4.2.1 and Figure 3.4.2.2 show crack growth rate (da/dN) *vs* stress-intensity factor range (ΔK) relationships for X60 and X80 steels in hydrogen gas [18, 19]. These relationships were measured at two gas pressures (5.5 and 21 MPa) and two R ratios (0.1 and 0.5) for each

steel. The general trends of the fatigue crack growth rates in Figure 3.4.2.1 and Figure 3.4.2.2 are similar to the trends in Figure 3.3.2.1, i.e., crack growth rates in hydrogen become increasingly greater relative to crack growth rates in air as ΔK increases. The magnitudes of the fatigue crack growth rates are also similar, as demonstrated by including data for A516 steel from Figure 3.3.2.1 in the plots for X60 and X80 in Figure 3.4.2.1 and Figure 3.4.2.2.

The effects of R ratio and gas pressure on the da/dN *vs* ΔK relationships for X60 and X80 steels are not readily established from the data in Figure 3.4.2.1 and Figure 3.4.2.2. In the higher ΔK range, increasing R ratio leads to modestly higher crack growth rates but varying gas pressure has essentially no effect on crack growth rates. In the lower ΔK range, the only clear trend for the X80 steel is that crack growth rates are highest in 21 MPa hydrogen gas at R=0.5. For the X60 steel at lower ΔK, crack growth rates appear higher for R=0.5 but the effect of gas pressure is not clear.

4. Fabrication

4.1 Heat treatment

Heat treating A516 steel to produce different microstructures does not significantly affect fatigue crack growth rates in hydrogen gas [14, 15]. The da/dN *vs* ΔK curves for A516 in three different heat treatment conditions (see Table 1.1.3) are plotted in Figure 4.1.1. The heat treatments produced the following three microstructures: ferrite plus pearlite with a 35 μm prior austenite grain size, ferrite plus pearlite with a 180 μm prior austenite grain size, and bainite plus continuous grain boundary ferrite with a 200 μm prior austenite grain size. The yield strengths of these microstructures are between 305 and 415 MPa (see Table 1.1.3). Despite the wide range in microstructures, the da/dN *vs* ΔK relationships are nearly identical at higher ΔK. The primary difference in the da/dN *vs* ΔK relationships is a mild shift in the threshold stress-intensity range (ΔK_{TH}) values, i.e., ΔK_{TH} varies from 8 to 11.5 MPa $\cdot m^{1/2}$ [14, 15].

An unexpected result was found when comparing the fatigue crack growth responses of X42 and 1080 steels in 6.9 MPa hydrogen gas [5]. The reduction of area (Table 3.1.1.1) and fracture toughness (Table 3.2.1.1) in hydrogen gas are lower for the 1080 steel compared to the X42 steel, but fatigue crack growth rates in 1080 steel are less affected by hydrogen gas. This is demonstrated from the da/dN *vs* ΔK relationships in Figure 4.1.2. It was suggested that hydrogen facilitates fatigue crack growth in the ferrite phase, so that fatigue crack growth rates are higher in the X42 steel with a ferrite plus pearlite microstructure compared to the 1080 steel with a fully pearlitic microstructure [5] .

4.2 Properties of welds

The tensile, fracture toughness, and fatigue crack growth properties of carbon steel welds have been measured in hydrogen gas. These properties are considered in the following paragraphs.

Tensile properties

A large amount of data has been generated for the tensile properties of carbon steel welds in 6.9 MPa hydrogen gas. Properties from both smooth and notched tensile specimens are summarized in Tables 4.2.1 through 4.2.4.

The trends for smooth tensile specimen properties of welds in hydrogen gas are similar to those for the base metals (section 3.1.1). Table 4.2.1 lists measurements from tensile specimens that were oriented perpendicular to the weld [4, 20]. Most reduction of area values range from 30 to 40%, which represent reduction of area losses of approximately 50% from values measured in air. These reduction of area properties were measured primarily for shielded metal arc and submerged arc welds. The lowest reduction of area values (12 to 20%) were measured for an electric resistance weld, a gas tungsten arc weld, and a gas metal arc weld. The weld with the reduction of area of 12% fractured in the transition zone between the heat affected zone and the base metal. Some of the highest reduction of area values measured (66 to 77%) were from specimens that fractured in the fusion zone.

Other smooth tensile specimens were tested in an orientation parallel to the weld, where the specimens were centered either in the fusion zone or heat affected zone. Table 4.2.2 shows that reduction of area values in hydrogen gas are mostly in the range 38 to 47% [20]. These values are generally greater than those measured from specimens oriented perpendicular to the weld.

Weld properties measured from notched tensile specimens in hydrogen gas are remarkably consistent, independent of specimen orientation relative to the weld. Tables 4.2.3 and 4.2.4 show that reduction of area values are in the range 9 to 17%, which represent reduction of area losses of 50 to 70% from values measured in air [4, 20]. In addition, hydrogen lowers the tensile strength by less than 15%. The reduction of area properties for welds are better than the properties reported for base metals (section 3.1.2) when measured using notched tensile specimens. The notched tensile strength properties for welds and base metals are similar.

Fracture toughness

The fracture toughness of welds in hydrogen gas depends on the type of weld and location of crack propagation, as summarized in Table 4.2.5. The fracture toughness and crack propagation resistance of submerged arc welds in X60 steel are high when crack propagation is in the fusion zone [8]. The fracture toughness of the weld fusion zone (103 $MPa \cdot m^{1/2}$) is equal to the fracture toughness of the base metal (Table 3.2.1.1). Furthermore, the crack propagation resistance of the weld fusion zone (267 MPa) exceeds the crack propagation resistance of the base metal (43 MPa, Table 3.2.1.1). In contrast, the fracture toughness of the heat affected zone was low and could not be measured reliably, since cracks ultimately propagated in a rapid, subcritical manner. The fracture toughness of the heat affected zone in electric resistance welded X42 was measured, and this value (48 $MPa \cdot m^{1/2}$) was lower than the fracture toughness of the base metal (107 $MPa \cdot m^{1/2}$, Table 3.2.1.1). No subcritical crack propagation was measured in the X42 weld heat affected zone when tested under static load in 6.9 MPa hydrogen gas [6].

Fatigue crack propagation

Welds in X60 steel are not more susceptible to fatigue crack growth than the base metal in 6.9 MPa hydrogen gas [14]. Figure 4.2.1 shows that the da/dN *vs* ΔK relationships for the fusion zone and heat affected zone of a submerged arc weld are nearly identical to the da/dN *vs* ΔK relationship for the base metal.

5. References

1. "Classification and Designation of Carbon and Low-Alloy Steels," in *Metals Handbook, Properties and Selection: Irons, Steels, and High-Performance Alloys*, 10th ed., vol. 1, ASM International, Materials Park OH, 1990, pp. 140-194.
2. VL Gadgeel and DL Johnson, "Gas-Phase Hydrogen Permeation and Diffusion in Carbon Steels as a Function of Carbon Content from 500 to 900 K," *Journal of Materials for Energy Systems*, vol. 1, 1979, pp. 32-40.
3. JP Hirth, "Effects of Hydrogen on the Properties of Iron and Steel," *Metallurgical Transactions A*, vol. 11A, 1980, pp. 861-890.
4. WR Hoover, JJ Iannucci, SL Robinson, JR Spingarn, and RE Stoltz, "Hydrogen Compatibility of Structural Materials for Energy Storage and Transmission," SAND80-8202, Sandia National Laboratories, Livermore, CA, 1980.
5. HJ Cialone and JH Holbrook, "Microstructural and Fractographic Features of Hydrogen-Accelerated Fatigue-Crack Growth in Steels," in *Microstructural Science: Welding, Failure Analysis, and Metallography*, vol. 14, MR Louthan, I LeMay, and GF VanderVoort, Eds., American Society for Metals, Metals Park, OH, 1987, pp. 407-422.
6. HJ Cialone and JH Holbrook, "Sensitivity of Steels to Degradation in Gaseous Hydrogen," in *Hydrogen Embrittlement: Prevention and Control, ASTM STP 962*, L Raymond, Ed., American Society for Testing and Materials, Philadelphia, 1988, pp. 134-152.
7. RJ Walter and WT Chandler, "Influence of Gaseous Hydrogen on Metals Final Report," NASA-CR-124410, NASA, Marshall Space Flight Center AL, 1973.
8. WR Hoover, SL Robinson, RE Stoltz, and JR Spingarn, "Hydrogen Compatibility of Structural Materials for Energy Storage and Transmission Final Report," SAND81-8006, Sandia National Laboratories, Livermore CA, 1981.
9. SL Robinson and RE Stoltz, "Toughness Losses and Fracture Behavior of Low Strength Carbon-Manganese Steels in Hydrogen," in *Hydrogen Effects in Metals*, IM Bernstein and AW Thompson, Eds., The Metallurgical Society of AIME, Warrendale, PA, 1981, pp. 987-995.
10. HJ Cialone and JH Holbrook, "Effects of Gaseous Hydrogen on Fatigue Crack Growth in Pipeline Steel," *Metallurgical Transactions A*, vol. 16A, 1985, pp. 115-122.
11. F Gutierrez-Solana and M Elices, "High-Pressure Hydrogen Behavior of a Pipeline Steel," in *Current Solutions to Hydrogen Problems in Steels*, CG Interrante and GM Pressouyre, Eds., American Society for Metals, Metals Park, OH, 1982, pp. 181-185.
12. AW Loginow and EH Phelps, "Steels for Seamless Hydrogen Pressure Vessels," *Corrosion*, vol. 31, 1975, pp. 404-412.
13. HG Nelson, "On the Mechanism of Hydrogen-Enhanced Crack Growth in Ferritic Steels," in *Proceedings of the Second International Conference on Mechanical Behavior of Materials*, ASM, Metals Park, OH, 1976, pp. 690-694.
14. HF Wachob, "The Influence of Microstructure on the Resistance of Low Strength Ferrous Alloys to Gas Phase Hydrogen Degradation," NASA-CR-166334, Failure Analysis Associates, Palo Alto, CA, 1981.
15. HF Wachob and HG Nelson, "Influence of Microstructure on the Fatigue Crack Growth of A516 in Hydrogen," in *Hydrogen Effects in Metals*, IM Bernstein and AW Thompson, Eds., The Metallurgical Society of AIME, Warrendale, PA, 1981, pp. 703-711.

16. RJ Walter and WT Chandler, "Cyclic-Load Crack Growth in ASME SA-105 Grade II Steel in High-Pressure Hydrogen at Ambient Temperature," in *Effect of Hydrogen on Behavior of Materials*, AW Thompson and IM Bernstein, Eds., The Metallurgical Society of AIME, Warrendale, PA, 1976, pp. 273-286.
17. HG Nelson, "Hydrogen-Induced Slow Crack Growth of a Plain Carbon Pipeline Steel Under Conditions of Cyclic Loading," in *Effect of Hydrogen on Behavior of Materials*, AW Thompson and IM Bernstein, Eds., The Metallurgical Society of AIME, Warrendale, PA, 1976, pp. 602-611.
18. C SanMarchi, BP Somerday, KA Nibur, DG Stalheim, T Boggess, and S Jansto, "Fracture and Fatigue of Commercial Grade API Pipeline Steels in Gaseous Hydrogen," in *Proceedings of the ASME 2010 Pressure Vessels & Piping Division / K-PVP Conference PVP2010*, Bellevue, Washington, 2010, PVP2010-25825.
19. D Stalheim, T Boggess, C SanMarchi, S Jansto, B Somerday, and G Muralidharan, "Microstructure and Mechanical Property Performance of Commercial Grade API Pipeline Steels in High Pressure Gaseous Hydrogen," in *Proceedings of IPC 2010 8th International Pipeline Conference*, Calgary, Alberta, 2010, IPC2010-31301.
20. WR Hoover, "Hydrogen Compatibility of Structural Materials for Energy Storage and Transmission," SAND79-8200, Sandia National Laboratories, Livermore, CA, 1979.
21. "Metals & Alloys in the Unified Numbering System," Standard SAE HS-1086/2004, 10th ed., SAE International, Warrendale, PA, 2004.
22. "Standard Specification for Seamless Carbon Steel Pipe for High-Temperature Service," Standard A 106/A 106M-04b, ASTM International, West Conshohocken PA, 2004.
23. "Standard Specification for Carbon Steel Forgings for Piping Applications," Standard A 105/A 105M-05, ASTM International, West Conshohocken, PA, 2005.
24. "Specification for Line Pipe," API Specification 5L, American Petroleum Institute, Washington DC, 1999.

Table 1.1.1. Allowable composition ranges (wt%) for carbon steels.

Steel	Specification	Fe	C	Mn	P	S	Si	Other	Ref.
A515 Gr. 70	UNS K03101	Bal	0.31 max	0.90 max	0.035 max	0.040 max	0.13 0.33	—	[21]
A516 Gr. 70	UNS K02700	Bal	0.27 max	0.79 1.30	0.035 max	0.040 max	0.13 0.45	—	[21]
A106 Gr. B	ASTM A106 (B)	Bal	0.30 max	0.29 1.06	0.035 max	0.035 max	0.10 min	—	[22]
A106 Gr. C	ASTM A106 (C)	Bal	0.35 max	0.29 1.06	0.035 max	0.035 max	0.10 min	—	[22]
SA 105 Gr. II	ASTM A105	Bal	0.35 max	0.60 1.05	0.035 max	0.040 max	0.10 0.35	—	[23]
1020	UNS G10200	Bal	0.18 0.23	0.30 0.60	0.030 max	0.050 max	—	—	[21]
1042	UNS G10420	Bal	0.40 0.47	0.60 0.90	0.030 max	0.050 max	—	—	[21]
1080	UNS G10800	Bal	0.75 0.88	0.60 0.90	0.030 max	0.050 max	—	—	[21]
X42†	API 5L X42	Bal	0.22 max	1.30 max	0.025 max	0.015 max	—	Nb+Ti+V<0.15	[24]
X52†	API 5L X52	Bal	0.22 max	1.40 max	0.025 max	0.015 max	—	Nb+Ti+V<0.15	[24]
X60†	API 5L X60	Bal	0.22 max	1.40 max	0.025 max	0.015 max	—	Nb+Ti+V<0.15‡	[24]
X65†	API 5L X65	Bal	0.22 max	1.45 max	0.025 max	0.015 max	—	Nb+Ti+V<0.15‡	[24]
X70†	API 5L X70	Bal	0.22 max	1.65 max	0.025 max	0.015 max	—	Nb+Ti+V<0.15‡	[24]
X80†	API 5L X80	Bal	0.22 max	1.85 max	0.025 max	0.015 max	—	Nb+Ti+V<0.15‡	[24]

† composition limits for welded product in Product Specification Level 2 (PSL 2)

‡ other compositions may be established by agreement between purchaser and manufacturer, but limit of Nb+Ti+V<0.15 must be satisfied

Table 1.1.2. Compositions (wt%) of carbon steels in hydrogen compatibility studies.

Steel	Product form	Fe	C	Mn	P	S	Si	Other	Ref.
A515 Gr. 70	0.95 cm plate	Bal	0.27	0.71	0.011	0.018	0.19	—	[7]
A516 Gr. 70	1.25 cm plate	Bal	0.22	1.10	0.009	0.023	0.21	—	[14, 15]
A516 Gr. 70	nr	Bal	0.24	1.12	0.013	0.022	0.21	<0.04 Al, Cr, Mo, Ni	[12]
A516 Gr. 70 (U.S. grade)	2.5 cm plate	Bal	0.21	1.04	0.012	0.020	0.21	—	[4, 8, 9, 20]
A516 (Japan grade)	plate	Bal	0.26	0.79	0.013	0.033	0.17	—	[4]
A106 Gr. B	pipeline	nr							[4, 20]
A106 Gr. C	nr	Bal	0.26	1.06	0.011	0.023	0.23	—	[12]
SA 105 Gr. II	59 cm OD, 37 cm ID hemisphere	Bal	0.23	0.62	0.010	0.015	0.15	—	[16]
1020	3.8 cm plate	nr							[13, 17]
1020	0.95 cm rod	Bal	0.17	0.47	0.011	0.037	—	—	[7]
1042	0.95 cm rod	Bal	0.44	0.76	0.008	0.020	0.20	—	[7]
1080	rail web section	Bal	0.85	0.79	0.007	0.042	0.173	—	[5]
X42	30.5 cm OD, 28.6 cm ID pipeline	Bal	0.26	0.82	0.020	0.026	0.014	<0.04 Cr, Cu, Mo, Ni ; <0.005 Al, Sn	[5, 6, 10]
X42	nr	Bal	0.10	0.70	0.033	0.022	0.26	0.17 Co, 0.15 Cr	[11]
X52	pipeline	Bal	0.14	0.98	0.015	0.012	0.29	<0.012 Al, Nb	[4, 20]
X60	pipeline	Bal	0.26	1.39	0.006	0.022	0.03	0.050 V	[4, 20]
X60	1.25 cm plate	Bal	0.12	1.29	0.014	0.016	0.25	<0.03 Cr, Cu, Mo, Nb, Ni, V	[8, 14]
X65	pipeline	Bal	0.22	1.23	—	—	0.11	0.020 Nb	[4, 20]
X70	101.6 cm OD, 98.6 ID pipeline	Bal	0.09	1.50	0.008	0.006	0.31	<0.42 Al, Cr, Cu, Mo; <0.084 Nb, Ni, Sn	[6]
X70	pipeline	Bal	0.11	1.44	0.013	0.002	0.27	<0.30 Cu, Ni; <0.09 Al, Nb, V	[4, 20]
X70 (Arctic grade)	pipeline	Bal	0.06	1.70	0.010	0.009	0.20	0.30 Mo, 0.062 Nb	[4, 20]
X60	plate	Bal	0.03	1.14	0.008	0.001	0.18	0.16 Cr, 0.14 Ni, 0.084 Nb, 0.034 Al, 0.014 Ti	[18, 19]
X80	plate	Bal	0.05	1.52	0.007	0.003	0.12	0.25 Cr, 0.14 Ni, 0.092 Nb, 0.036 Al, 0.012 Ti	[18, 19]

nr = not reported; ID = inner diameter; OD = outer diameter

Table 1.1.3. Heat treatments and mechanical properties of carbon steels in hydrogen compatibility studies.

Steel	Heat treatment	S_y (MPa)	S_u (MPa)	RA (%)	Ref.
A515 Gr. 70	HR	338	504	66	[7]
A516 Gr. 70 (F+P, GS = 35 μm)	N 1173 K/45 min + FC	330	565	—	[14, 15]
A516 Gr. 70 (F+P, GS = 180 μm)	N 1473 K/45 min + FC	305	—	—	
A516 Gr. 70 (B, GS = 200 μm)	A 1473 K/45 min + ISQ + T 723 K/90 min	415	—	—	
A516 Gr. 70	HR	290	572	62	[12]
A516 Gr. 70 (U.S. grade)	HR	375	535	69	[4, 8, 9, 20]
A516 (Japan grade)	nr	364	566	72	[4]
A106 Gr. B	nr	462	559	58	[4, 20]
A106 Gr. C	N 1130 K/75 min + AC	345	558	68	[12]
SA 105 Gr. II	SR 894 K/240 min + 0.9 K/min cool	269	462	63	[16]
1020	HR	207	379	—	[13, 17]
1020	HR	373	490	65	[7]
1042	N 1172 K/60 min + AC	400†	621†	59†	[7]
1080	N 1123 K/60 min + FC	414†	814†	16†	[5]
X42	HR	366	511	56	[5, 6, 10]
X42	nr	280	415	58	[11]
X52	nr	414	609	60	[4, 20]
X60	nr	427	594	49	[4, 20]
X60	nr	473	675	62	[8, 14]
X65	nr	504	605	57	[4, 20]
X70	CR	584	669	57	[6]
X70	nr	626	693	77	[4, 20]
X70 (Arctic grade)	nr	697	733	77	[4, 20]
X60	nr	434	486	88†	[18, 19]
X80	nr	565	600	81†	[18, 19]

nr = not reported; A = austenitize; AC = air cool; B = bainite; CR = controlled rolled; F = ferrite; FC = furnace cool; GS = grain size; ISQ = isothermal quench; HR = hot rolled; N = normalized; P = pearlite; SR = stress relief

† properties measured in high-pressure nitrogen or helium gas

Table 2.1. Hydrogen permeability (Φ) and solubility (S) *vs* temperature relationships for carbon steels and iron.*

Material	Temp. range (K)	Pressure range (MPa)	$\Phi = \Phi_o \exp(-E_\Phi / RT)$		$S = S_o \exp(-E_S / RT)$		Ref.
			Φ_o $\left(\frac{\text{mol H}_2}{\text{m} \cdot \text{s} \cdot \text{MPa}^{1/2}}\right)$	E_Φ $\left(\frac{\text{kJ}}{\text{mol}}\right)$	S_o $\left(\frac{\text{mol H}_2}{\text{m}^3 \cdot \text{MPa}^{1/2}}\right)$	E_S $\left(\frac{\text{kJ}}{\text{mol}}\right)$	
Iron	500 - 900	0.01 - 0.7	2.513×10^{-5}	31.69	180.1	23.66	[2]
1010			3.442×10^{-5}	34.18	202.4	24.70	
1020			3.77×10^{-5}	35.07	159.0	23.54	
1035			3.603×10^{-5}	36.16	188.6	24.63	
1050			2.097×10^{-5}	34.13	82.89	21.10	
1065			1.602×10^{-5}	34.73	65.63	21.54	
1095			1.039×10^{-5}	33.43	41.98	19.28	

* Diffusivity (D) can be obtained from the ratio of permeability and solubility, i.e., $D = \Phi / S$

Table 3.1.1.1. Smooth tensile properties of carbon steels in 6.9 MPa hydrogen gas at room temperature. Properties in either air or nitrogen gas are included for comparison. The tensile specimen orientation is longitudinal (L) unless otherwise specified.

Steel	Test environment	Strain rate (s^{-1})	S_y (MPa)	S_u (MPa)	El_t (%)	RA (%)	Ref.
A516 (U.S. grade)	Air 6.9 MPa H_2	~ $3x10^{-4*}$	375 364	535 551	17 19	69 43	[4]
A516 (Japan grade)	Air 6.9 MPa H_2	~ $3x10^{-4*}$	364 359	566 571	22 18	72 37	[4]
A106 Gr. B	Air 6.9 MPa H_2	~ $3x10^{-4*}$	462 503	559 576	14 11	58 50	[4]
1080	6.9 MPa N_2 6.9 MPa H_2	$1x10^{-4}$	414 421	814 794	12 7.5	16 7.2	[5]
1080 (T)	6.9 MPa N_2 6.9 MPa H_2		414 407	814 787	10 7.4	14 6.5	
X42	Air 6.9 MPa H_2	$1x10^{-4}$	366 331	511 483	21 20	56 44	[5, 6, 10]
X42 (T)	Air 6.9 MPa H_2		311 338	490 476	21 19	52 41	
X52	Air 6.9 MPa H_2	~ $3x10^{-4*}$	414 429	609 597	19 15	60 37	[4]
X60	Air 6.9 MPa H_2	~ $3x10^{-4*}$	427 422	594 590	13 10	49 27	[4]
X65	Air 6.9 MPa H_2	~ $3x10^{-4*}$	504 506	605 611	15 15	57 36	[4]
X70	Air 6.9 MPa H_2	$1x10^{-4}$	584 548	669 659	20 20	57 47	[6]
X70 (T)	Air 6.9 MPa H_2		613 593	702 686	19 15	53 38	
X70	Air 6.9 MPa H_2	~ $3x10^{-4*}$	626 566	693 653	16 14	77 37	[4]
X70 (Arctic grade)	Air 6.9 MPa H_2	~ $3x10^{-4*}$	697 695	733 733	14 12	77 37	[4]

T = transverse oriented specimen

* calculated based on displacement rate and specimen gauge length

Table 3.1.1.2. Smooth tensile properties of carbon steels in 69 MPa hydrogen gas at room temperature. Properties in air and/or helium gas are included for comparison.

Steel	Test environment	Strain rate* (s^{-1})	S_y (MPa)	S_u (MPa)	El_t (%)	RA (%)	Ref.
1042	69 MPa He 69 MPa H_2	$3.3x10^{-5}$	400† -	621 614	29 22	59 27	[7]
1020‡	Air 69 MPa He 69 MPa H_2	$3.3x10^{-5}$	373† 283† 276†	490 435 428	— 40 32	65 68 45	[7]
A515	Air 69 MPa He 69 MPa H_2	$3.3x10^{-5}$	338† 276† 297†	504 448 442	— 42 29	66 67 35	[7]

* strain rate in elastic range
† defined at deviation from linearity on load *vs* time plot
‡ prestrained under tension in air immediately prior to testing

Table 3.1.2.1. Notched tensile properties of carbon steels in 6.9 MPa hydrogen gas at room temperature. Properties in air are included for comparison.

Steel	Specimen	Test environment	Displ. rate (mm/s)	S_y* (MPa)	σ_s (MPa)	RA (%)	Ref.
A516 (U.S. grade)	(a)	Air 6.9 MPa H_2	$8.5x10^{-3}$	375 364	759 629	30 5.4	[4]
A106 Gr. B	(a)	Air 6.9 MPa H_2	$8.5x10^{-3}$	462 503	618 619	26 8.0	[4]
X52	(a)	Air 6.9 MPa H_2	$8.5x10^{-3}$	414 429	818 707	15 7.0	[4]
X60	(a)	Air 6.9 MPa H_2	$8.5x10^{-3}$	427 422	847 782	23 8.4	[4]
X65	(a)	Air 6.9 MPa H_2	$8.5x10^{-3}$	504 506	806 758	21 6.1	[4]
X70	(a)	Air 6.9 MPa H_2	$8.5x10^{-3}$	626 566	946 845	45 8.7	[4]
X70 (Arctic grade)	(a)	Air 6.9 MPa H_2	$8.5x10^{-3}$	697 695	1027 949	42 8.6	[4]

* yield strength of smooth tensile specimen
(a) V-notched specimen: 90^o included angle; minimum diameter = 2.44 mm; maximum diameter = 2.87 mm; notch root radius = 0.025 to 0.051 mm.

Table 3.1.2.2. Notched tensile properties of carbon steels in 69 MPa hydrogen gas at room temperature. Properties in air and/or helium gas are included for comparison.

Steel	Specimen	Test environment	Displ. rate (mm/s)	S_y* (MPa)	σ_s (MPa)	RA (%)	Ref.
1042	(a)	69 MPa He 69 MPa H_2	~ $4x10^{-4}$	400 —	1056 793	8.5 2.8	[7]
1020§	(a)	Air 69 MPa He 69 MPa H_2	~ $4x10^{-4}$	373 283 276	787 724 621	12 14 8.3	[7]
A515	(a)	69 MPa He 69 MPa H_2	~ $4x10^{-4}$	276 297	731 559	8.1 2.3	[7]

* yield strength of smooth tensile specimen

(a) V-notched specimen: 60^o included angle; minimum diameter = 3.81 mm; maximum diameter = 7.77 mm; notch root radius = 0.024 mm. Nominal stress concentration factor (K_t) = 8.4.

Table 3.2.1.1. Fracture toughness for carbon steels in hydrogen gas at room temperature. The fracture toughness in air, nitrogen, or helium is included for comparison. The crack propagation direction is parallel to the longitudinal orientation of the material product form.

Steel	S_y † (MPa)	RA† (%)	Test environment	Displ. rate (mm/s)	K_{Ic} (MPa $\cdot m^{1/2}$)	K_{IH} ‡ (MPa $\cdot m^{1/2}$)	dJ/da (MPa)	Ref.
A516	375	69	Air 3.5 MPa H_2 6.9 MPa H_2 20.7 MPa H_2 34.5 MPa H_2	$8.5x10^{-3}$	166*	 131 113 98 90	516 47 55 54 57	[8, 9]
1080	414	16	6.9 MPa N_2 6.9 MPa H_2	$2.5x10^{-4}$ - $2.5x10^{-3}$	111	 81	42 13	[5]
X42	366	56	6.9 MPa N_2 6.9 MPa H_2	$2.5x10^{-4}$ - $2.5x10^{-3}$	178*	 107	70 63	[5, 6, 10]
X42	280	58	Air 2.0 MPa H_2 4.0 MPa H_2 6.5 MPa H_2 7.0 MPa H_2 8.0 MPa H_2 10.0 MPa H_2 12.2 MPa H_2 16.0 MPa H_2	$\leq 3.3x10^{-4}$	147*	 101-128 85 69 73# 59# 53# 57# 46#	111 — 36 31 — — — — —	[11]
X60	473	62	6.9 MPa He 6.9 MPa H_2	$8.5x10^{-3}$	142	 104	123 43	[8]
X70	584	57	6.9 MPa N_2 6.9 MPa H_2	$2.5x10^{-4}$ - $2.5x10^{-3}$	197	 95	251 23	[6]
X60	434	88	5.5 MPa H_2 21 MPa H_2	$8.3x10^{-5}$ - $8.3x10^{-4}$	—	85 82	—	[18]
X80	565	81	5.5 MPa H_2 21 MPa H_2	$8.3x10^{-5}$ - $8.3x10^{-4}$	—	105 102	—	[18]

† yield strength and reduction of area of smooth tensile specimen in air

‡ calculated from relationship $K = \sqrt{JE/1-\nu^2}$

* reported fracture toughness may not be valid plane strain measurement

\# measured from burst tests on pipes with machined flaws

Table 3.2.2.1. Threshold stress-intensity factor for carbon steels in high-pressure hydrogen gas at 286 K. The crack propagation direction is parallel to the longitudinal orientation of the material product form.

Steel	S_y† (MPa)	RA† (%)	K_{Ic}† (MPa ·$m^{1/2}$)	Test environment	K_{TH} (MPa ·$m^{1/2}$)	Ref.
A516	290	62	*	69 MPa H_2	NCP 82	[12]
A106 Gr. C	345	68	*	97 MPa H_2	NCP 55	[12]

NCP = no crack propagation
† properties measured in air
* specimen dimensions precluded valid measurement

Table 4.2.1. Smooth tensile properties of carbon steel welds in 6.9 MPa hydrogen gas at room temperature. Properties in air are included for comparison. The tensile specimen orientation is perpendicular to the weld.

Steel / Weld	Test environment	Strain rate (s^{-1})	S_y (MPa)	S_u (MPa)	El_t (%)	RA (%)	Fracture location	Ref.
A106 Gr. B / SMA	Air 6.9 MPa H_2	~ $3x10^{-4}$*	393 385	615 553	21 14	77 40	nr	[4]
X52 / ERW	Air 6.9 MPa H_2	~ $3x10^{-4}$*	513 499	633 621	10 6.1	40 20	nr	[4]
X65 / SA	Air 6.9MPa H_2	~ $3x10^{-4}$*	516 505	633 624	13 10	56 30	nr	[4]
X70 / SA (Arctic grade)	Air 6.9 MPa H_2	~ $3x10^{-4}$*	649 643	686 678	12 9.5	69 37	nr	[4]
A516 / SMA	Air Air 6.9 MPa H_2 6.9 MPa H_2 6.9 MPa H_2 6.9 MPa H_2	nr	338 386 366 373 462 435	531 545 524 545 531 552	23 13 17 18 14 12	72 69 31 48 77 66	BM FZ BM FZ FZ FZ	[20]
A516 / GTA	Air 6.9 MPa H_2 6.9 MPa H_2	nr	435 435 462	593 593 580	16 15 6	71 38 20	BM BM FZ	[20]
A516 / GMA	Air 6.9 MPa H_2	nr	373 386	573 517	23 3	73 12	FZ TZ	[20]

nr = not reported; BM = base metal; ERW = electric resistance weld; FZ = fusion zone; GMA = gas metal arc; GTA = gas tungsten arc; SA = submerged arc; SMA = shielded metal arc; TZ = transition zone
* calculated based on displacement rate and specimen gauge length

Table 4.2.2. Smooth tensile properties of A516 steel welds in 6.9 MPa hydrogen gas at room temperature. Properties in air are included for comparison. The tensile specimen orientation is parallel to the weld.

Steel / Weld	Test environment	Strain rate (s^{-1})	S_y (MPa)	S_u (MPa)	El_t (%)	RA (%)	Specimen location	Ref.
A516 / SMA	Air	nr	424	505	25	82	FZ	[20]
	Air		483	593	13	66	HAZ	
	6.9 MPa H_2		444	528	15	46	FZ	
	6.9 MPa H_2		386	559	15	38	HAZ	
A516 / GTA	Air	nr	600	690	13	67	FZ	[20]
	Air		421	566	26	64	HAZ	
	6.9 MPa H_2		517	600	8.7	44	FZ	
	6.9 MPa H_2		497	600	15	58	HAZ	
A516 / GMA	Air	nr	600	690	17	67	FZ	[20]
	Air		331	559	27	70	HAZ	
	6.9 MPa H_2		580	676	11	42	FZ	
	6.9 MPa H_2		407	566	18	47	HAZ	

nr = not reported; FZ = fusion zone; GMA = gas metal arc; GTA = gas tungsten arc; HAZ = heat affected zone; SMA = shielded metal arc

Table 4.2.3. Notched tensile properties of carbon steel welds in 6.9 MPa hydrogen gas at room temperature. Properties in air are included for comparison. The notched tensile specimen orientation is perpendicular to the weld.

Steel / Weld	Specimen	Test environment	Displ. rate (mm/s)	S_y* (MPa)	σ_s (MPa)	RA (%)	Ref.
A106 Gr. B / SMA	(a)	Air	$8.5x10^{-3}$	393	719	49	[4]
		6.9 MPa H_2		385	603	14	
X70 / SA (Arctic grade)	(a)	Air	$8.5x10^{-3}$	649	1002	35	[4]
		6.9 MPa H_2		643	973	10	
X70 / SMA (Arctic grade)	(a)	Air	$8.5x10^{-3}$	551	1025	20	[4]
		6.9 MPa H_2		595	901	9.0	

SA = submerged arc; SMA = shielded metal arc

* yield strength of smooth tensile specimen

(a) V-notched specimen: 90^o included angle; minimum diameter = 2.44 mm; maximum diameter = 2.87 mm; notch root radius = 0.025 to 0.051 mm.

Table 4.2.4. Notched tensile properties of A516 steel welds in 6.9 MPa hydrogen gas at room temperature. Properties in air are included for comparison. The notched tensile specimen orientation is parallel to the weld.

Steel / Weld	Specimen	Test environment	Displ. rate (mm/s)	S_y* (MPa)	σ_s (MPa)	RA (%)	Specimen location	Ref.
A516 / SMA	(a)	Air	nr	424	738	62	FZ	[20]
		Air		483	828	32	HAZ	
		6.9 MPa H_2		444	642	10	FZ	
		6.9 MPa H_2		386	842	17	HAZ	
A516 / GTA	(a)	Air	nr	600	945	36	FZ	[20]
		Air		421	821	32	HAZ	
		6.9 MPa H_2		517	800	17	FZ	
		6.9 MPa H_2		497	697	9	HAZ	
A516 / GMA	(a)	Air	nr	600	945	25	FZ	[20]
		Air		331	780	34	HAZ	
		6.9 MPa H_2		580	835	12	FZ	
		6.9 MPa H_2		407	655	10	HAZ	

nr = not reported; FZ = fusion zone; GMA = gas metal arc; GTA = gas tungsten arc; HAZ = heat affected zone; SMA = shielded metal arc

* yield strength of smooth tensile specimen

(a) V-notched specimen: 90^o included angle; minimum diameter = 2.27 mm; maximum diameter = 2.87 mm; notch root radius = 0.051 mm.

Table 4.2.5. Fracture toughness for carbon steel welds in hydrogen gas at room temperature. The fracture toughness in nitrogen or helium is included for comparison.

Steel / Weld	S_y † (MPa)	Test environment	Displ. rate (mm/s)	K_{Ic} ‡ (MPa ·$m^{1/2}$)	K_{IH} ‡ (MPa ·$m^{1/2}$)	dJ/da (MPa)	Specimen location	Ref.
X42 / ERW	366	6.9 MPa N_2 6.9 MPa H_2	$2.5x10^{-4}$ - $2.5x10^{-3}$	67	48	97 69	HAZ HAZ	[6]
X60 / SA (1 pass)	473	6.9 MPa He 6.9 MPa He 6.9 MPa H_2 6.9 MPa H_2	$8.5x10^{-3}$	188* 205*	103 109#	452 171 267 §	FZ HAZ FZ HAZ	[8]
X60 / SA (2 pass)		6.9 MPa He 6.9 MPa He 6.9 MPa H_2 6.9 MPa H_2		188* 77	103 §	452 253 267 §	FZ HAZ FZ HAZ	

ERW = electric resistance weld; FZ = fusion zone; HAZ = heat affected zone;
SA = submerged arc

† yield strength of base metal from smooth tensile specimen in air

‡ calculated from relationship $K = \sqrt{JE/1-\nu^2}$

* reported fracture toughness may not be valid plane strain measurement

\# calculated from J-integral value at onset of rapid, subcritical crack extension

§ not measured due to rapid, subcritical crack extension

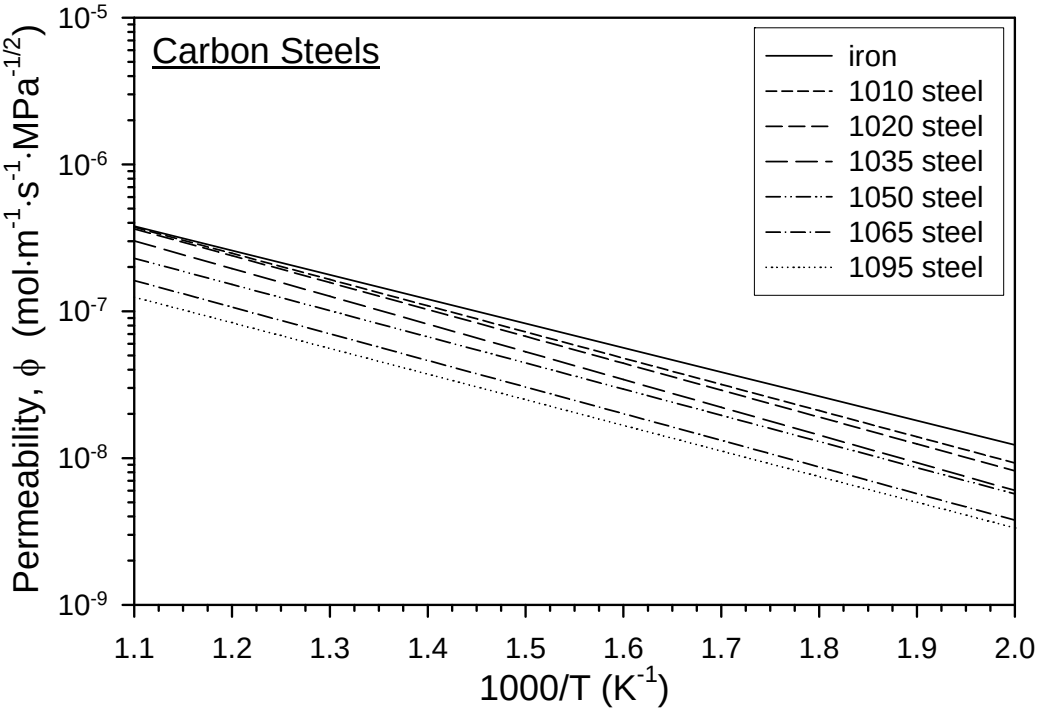

Figure 2.1. Permeability *vs* temperature relationships for carbon steels and iron [2].

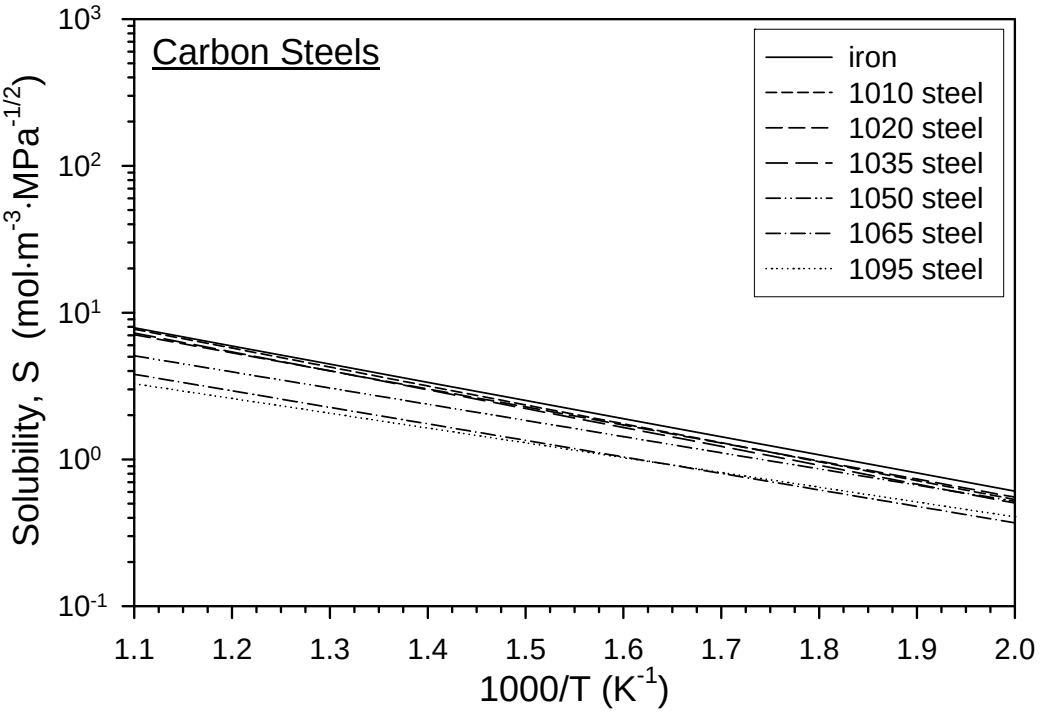

Figure 2.2. Solubility *vs* temperature relationships determined from permeability and diffusivity *vs* temperature relationships for carbon steels and iron [2].

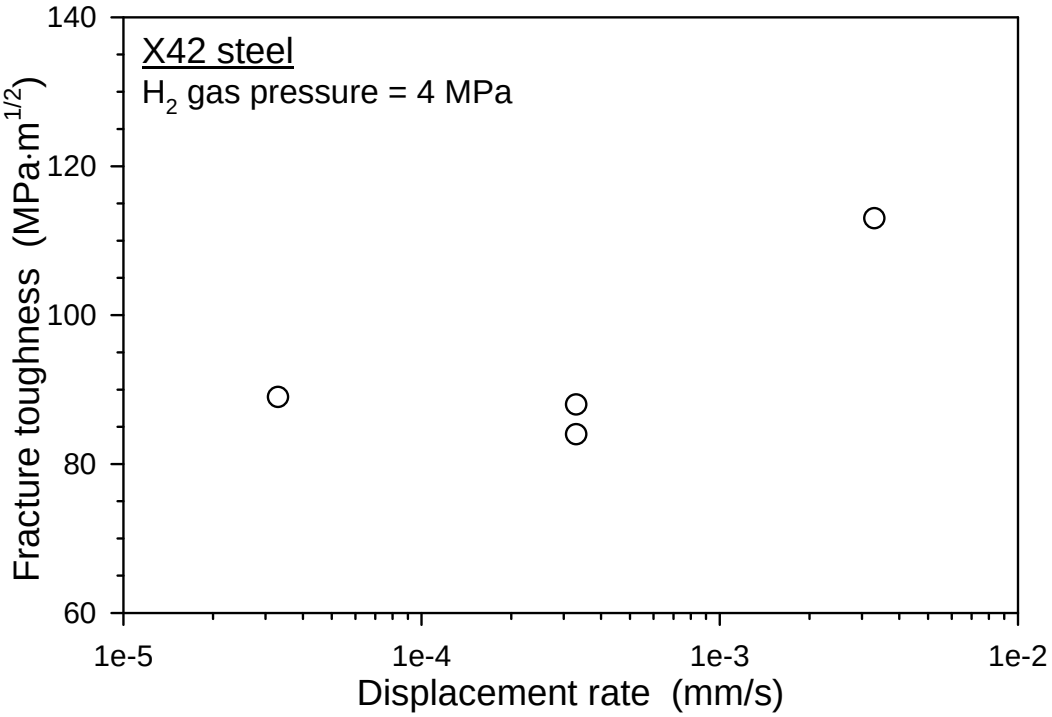

Figure 3.2.1.1. Effect of displacement rate on fracture toughness in hydrogen gas for X42 steel [11].

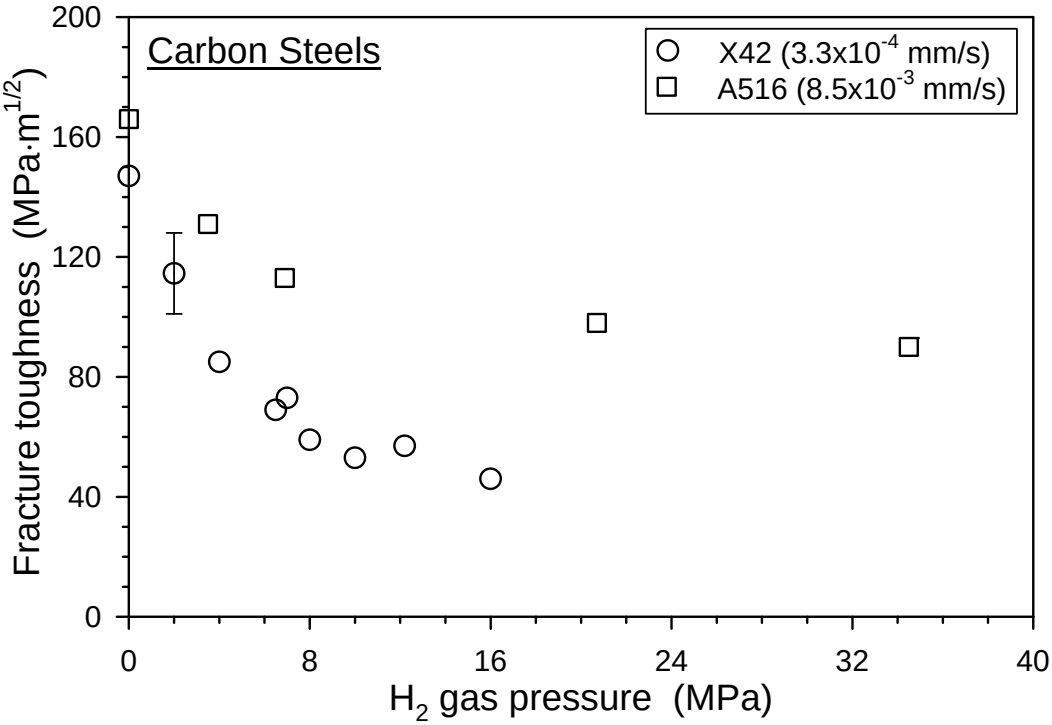

Figure 3.2.1.2. Effect of hydrogen gas pressure on fracture toughness for carbon steels [8, 9, 11]. The displacement rate used in the fracture toughness tests is indicated for each steel.

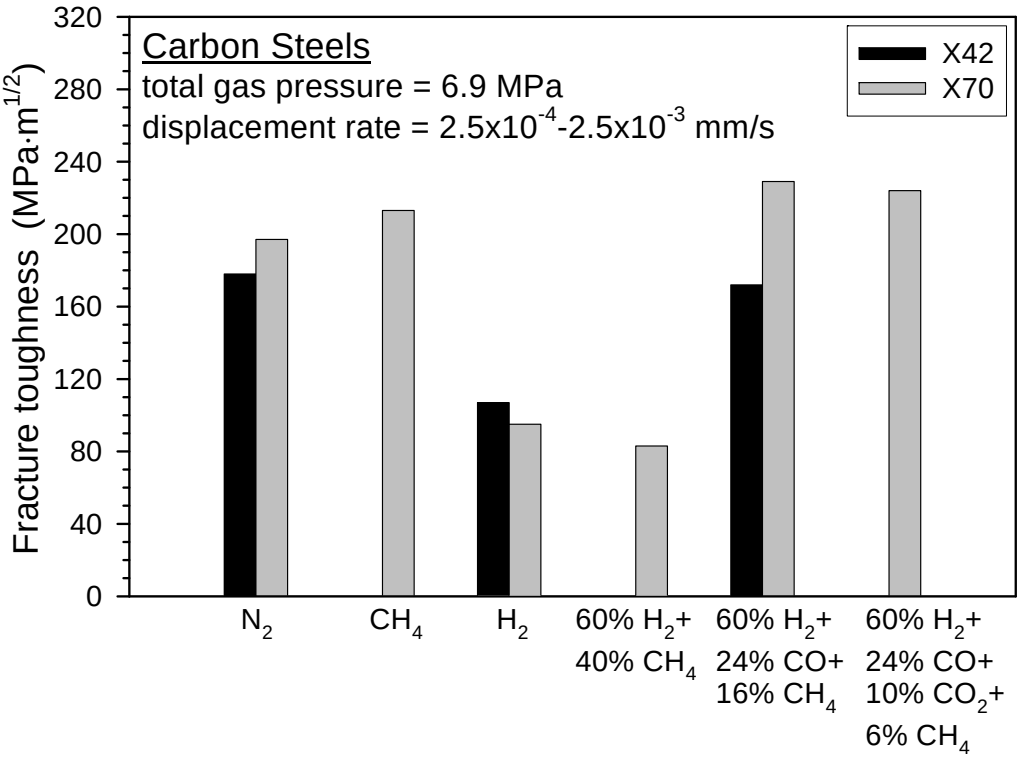

Figure 3.2.1.3. Effect of gas composition on fracture toughness for carbon steels [6].

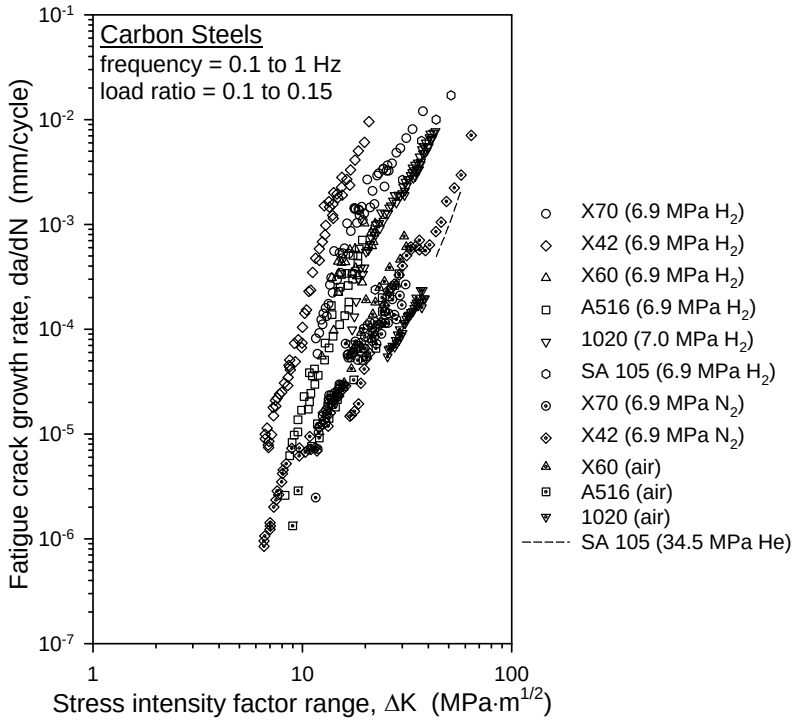

Figure 3.3.2.1. Fatigue crack growth rate *vs* stress-intensity factor range relationships for carbon steels in hydrogen gas [6, 10, 13-16]. Fatigue crack growth rate data in air, nitrogen, or helium are included for comparison.

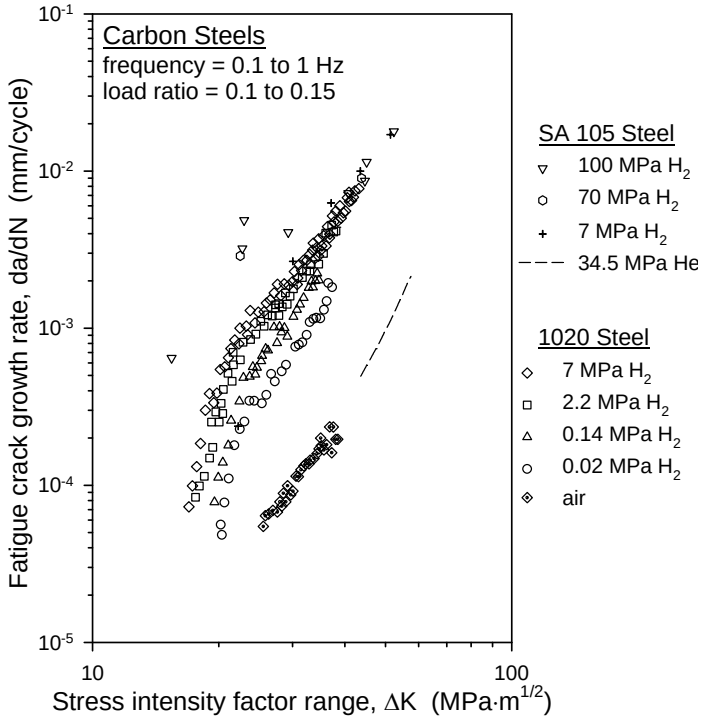

Figure 3.3.2.2. Effect of hydrogen gas pressure on fatigue crack growth rate *vs* stress-intensity factor range relationships for carbon steels [13, 16]. Fatigue crack growth rate data in air or helium gas are included for comparison.

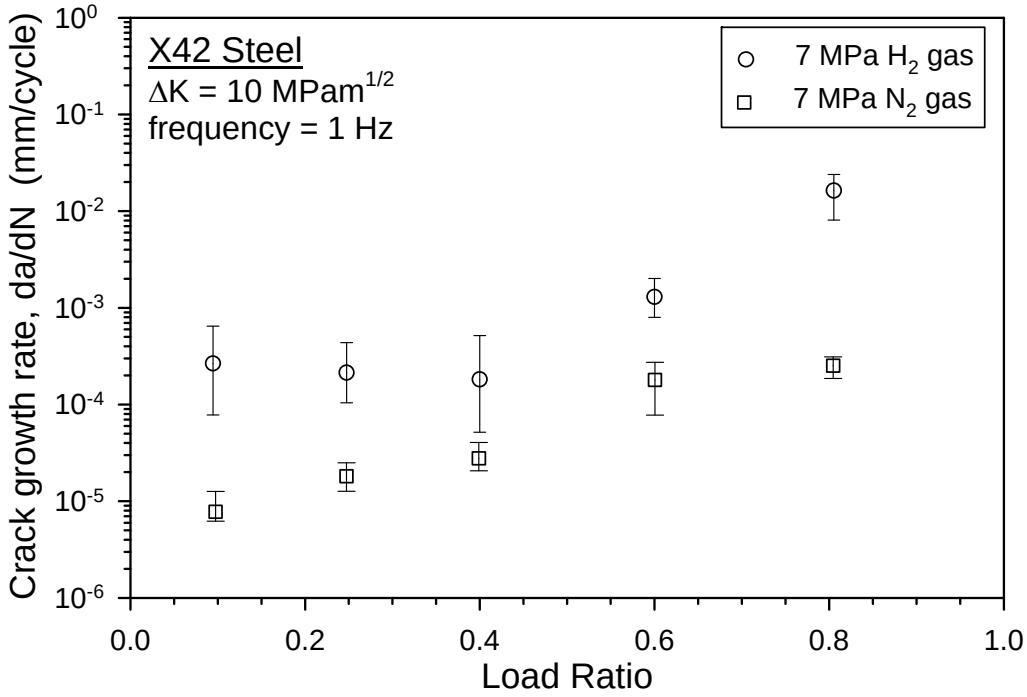

Figure 3.3.2.3. Effect of load ratio on fatigue crack growth rate for X42 steel in hydrogen gas at fixed stress-intensity factor range [10]. Fatigue crack growth rate data in nitrogen gas are included for comparison.

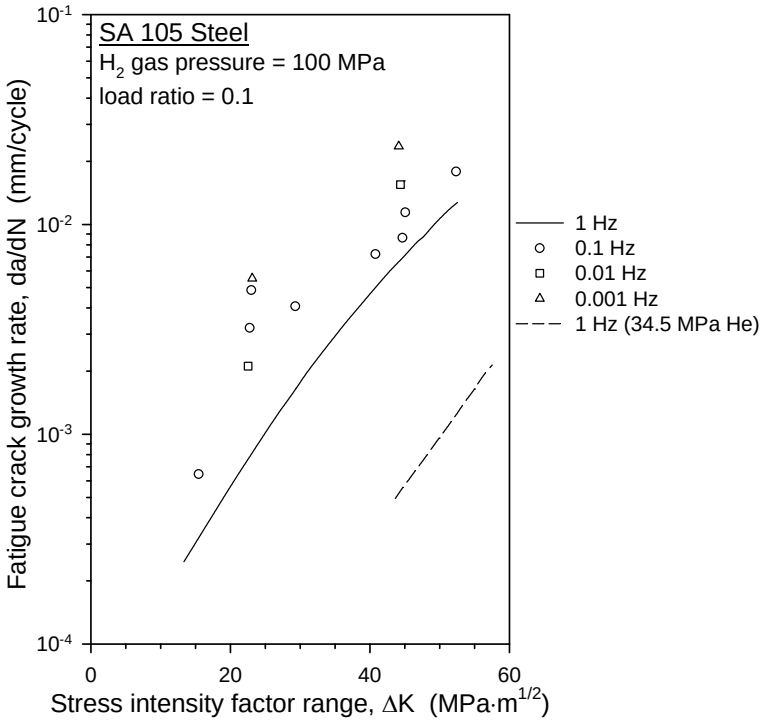

Figure 3.3.2.4. Effect of load cycle frequency on fatigue crack growth rate *vs* stress-intensity factor range relationships for SA 105 steel in hydrogen gas [16]. Fatigue crack growth rate data in helium gas are included for comparison.

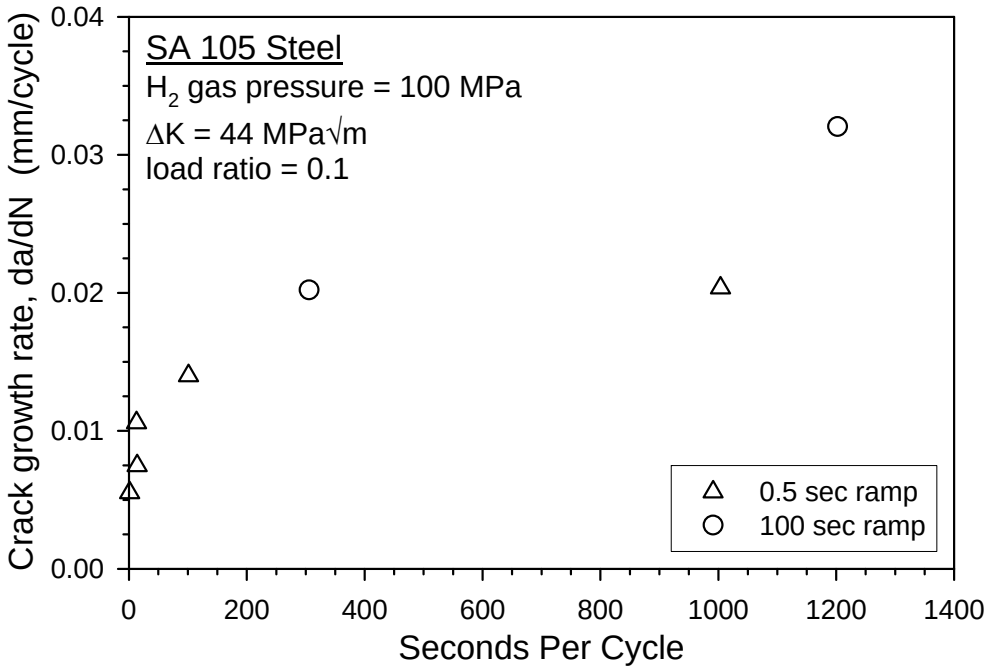

Figure 3.3.2.5. Effect of load cycle duration on fatigue crack growth rate for SA 105 steel in hydrogen gas at fixed stress-intensity factor range [16]. Data for two different loading ramp rates are displayed.

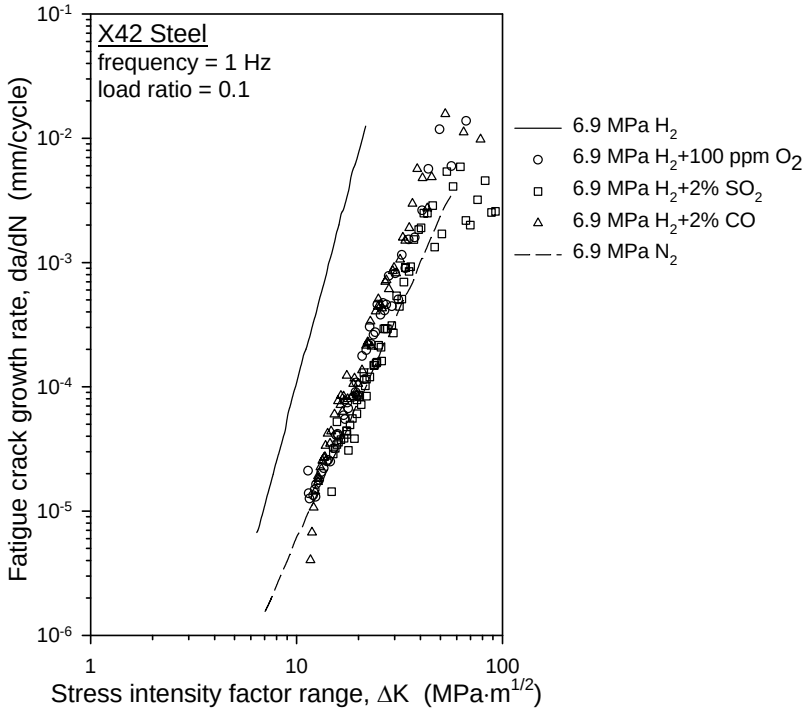

Figure 3.3.2.6. Effect of hydrogen gas composition on fatigue crack growth rate *vs* stress-intensity factor range relationships for X42 steel [6]. Fatigue crack growth rate data in nitrogen gas are included for comparison.

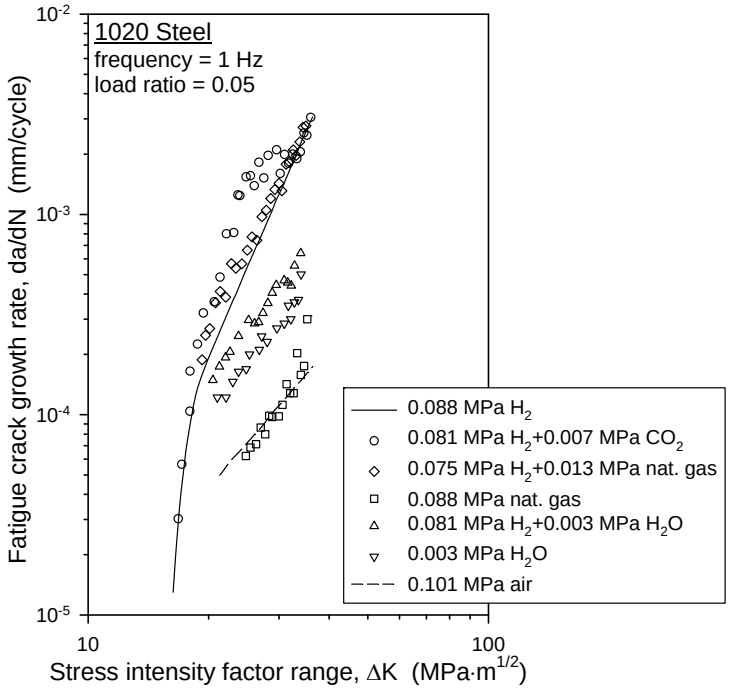

Figure 3.3.2.7. Effect of gas composition on fatigue crack growth rate *vs* stress-intensity factor range relationships for 1020 steel in low-pressure hydrogen gas [17]. Fatigue crack growth rate data in natural gas, water, and air are included for comparison.

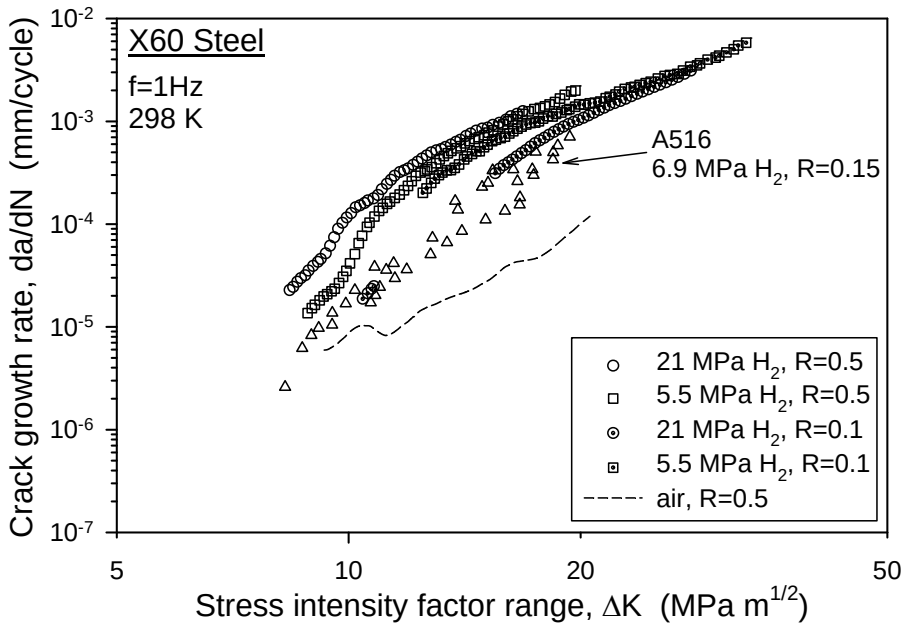

Figure 3.4.2.1. Fatigue crack growth rate *vs* stress-intensity factor range relationships for X60 steel in hydrogen gas [18]. These relationships were measured at two gas pressures and two R ratios. Two additional sets of data are included for comparison: data for X60 in air and data for A516 steel in hydrogen gas from Figure 3.3.2.1.

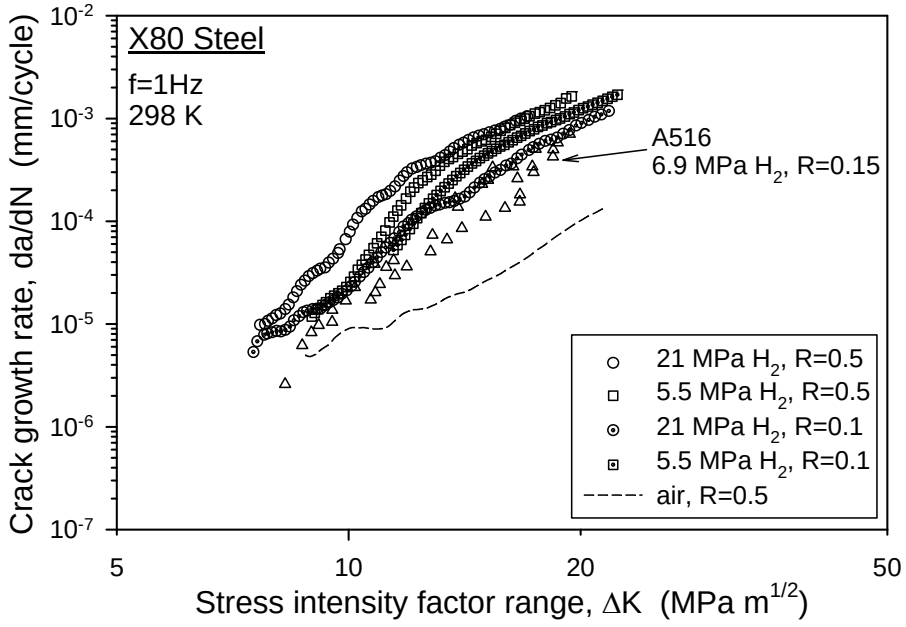

Figure 3.4.2.2. Fatigue crack growth rate *vs* stress-intensity factor range relationships for X80 steel in hydrogen gas [18]. These relationships were measured at two gas pressures and two R ratios. Two additional sets of data are included for comparison: data for X80 in air and data for A516 steel in hydrogen gas from Figure 3.3.2.1.

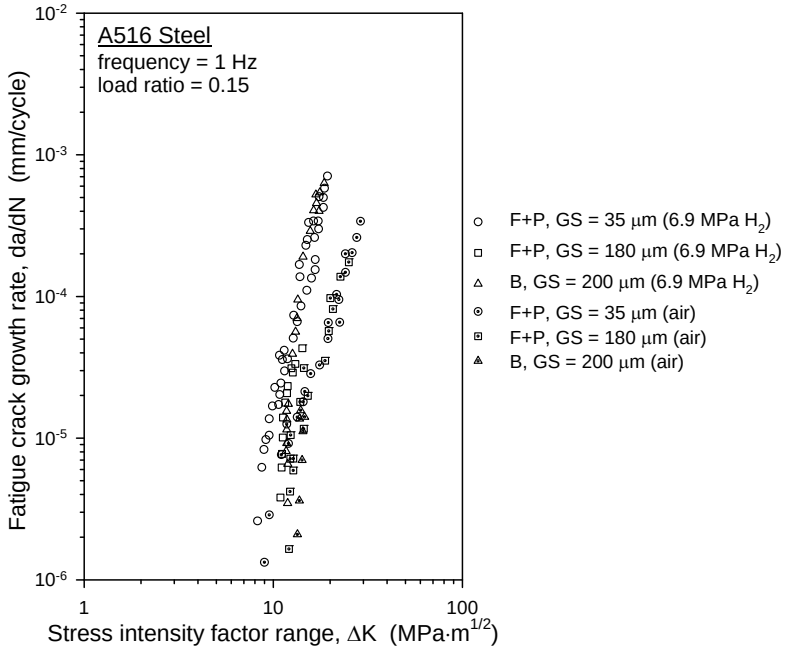

Figure 4.1.1. Effect of microstructure on fatigue crack growth rate *vs* stress-intensity factor range relationships for A516 steel in hydrogen gas [15]. Data are shown for both ferrite plus pearlite and bainitic microstructures at different grain sizes. Fatigue crack growth rate data in air are included for comparison. B = bainite; F = ferrite; GS = grain size; P = pearlite.

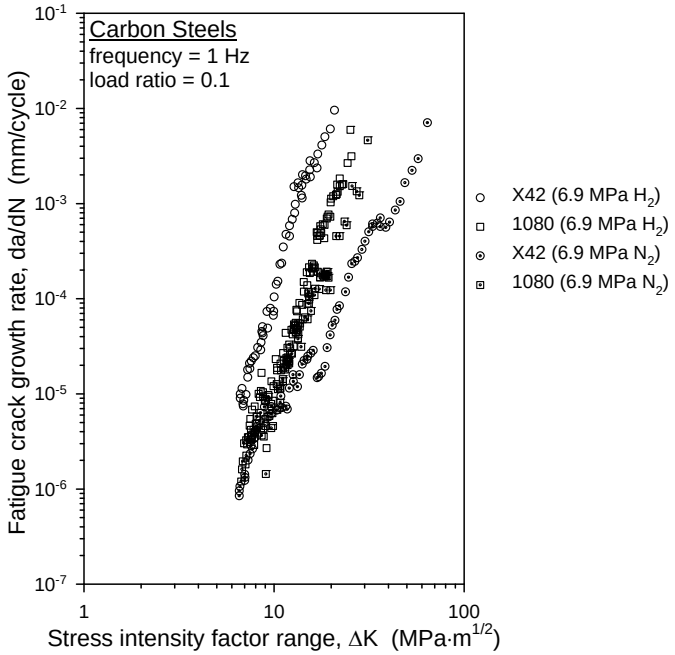

Figure 4.1.2. Effect of microstructure on fatigue crack growth rate *vs* stress-intensity factor range relationships for carbon steels in hydrogen gas [5]. Fatigue crack growth rate data in nitrogen gas are included for comparison.

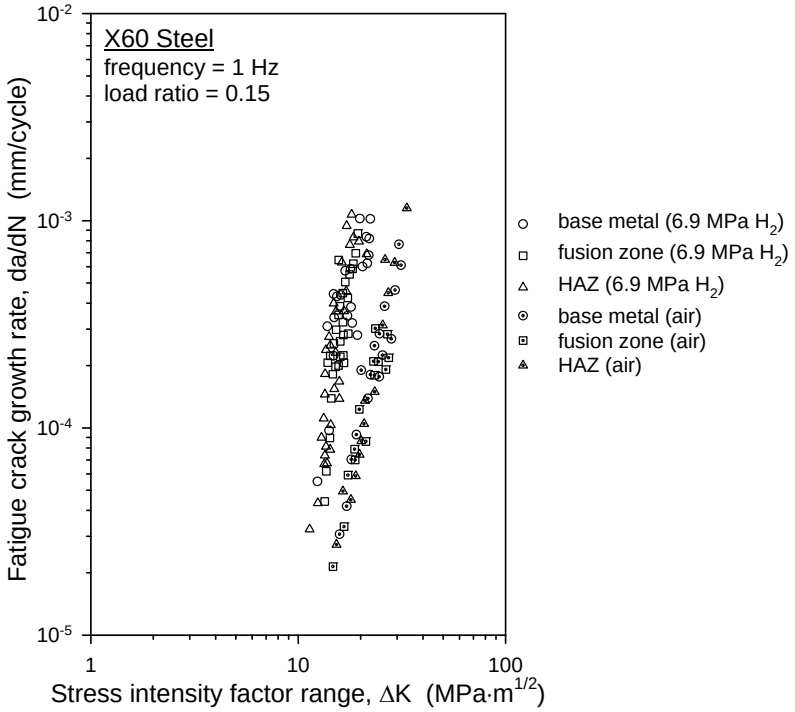

Figure 4.2.1. Fatigue crack growth rate *vs* stress-intensity factor range relationships for welded X60 steel in hydrogen gas [14]. Data are shown for both the fusion zone and heat-affected zone of the weld as well as the base metal. Fatigue crack growth rate data in air are included for comparison.